Journal of Superconductivity and Novel Magnetism (2022) 35:851–856
https://doi.org/10.1007/s10948-021-06119-y

ORIGINAL PAPER

Characteristics of Thin Films of Ferromagnetic Semiconductor $Fe_{1.1}Ti_{0.9}O_{3-\delta}$ Under the Pulsed Laser Deposition Method at Different Substrate Temperatures

Jialing Xu[1] · Ying Su[2,3] · Liyun Jia[1,2] · Li Ma[2] · Ping Song[2] · Lingjun Zhao[1] · Pu Liu[1] · Tao Wang[1] · Denglu Hou[2]

Received: 17 November 2021 / Accepted: 6 December 2021 / Published online: 29 January 2022

Abstract
In this study, epitaxial $Fe_{1.1}Ti_{0.9}O_{3-\delta}$ thin films with a smooth surface were prepared by adjusting the substrate temperature (T_S) and via pulsed laser deposition (PLD) in Ar gas and α-Al_2O_3 (001) substrate. During the study of the optical properties and magnetism of the thin film samples, it was established that all thin films grown in Ar gas were hypoxic, having more oxygen vacancies and widening the optical band gap of the thin films significantly. The substrate temperature has a significant effect on the crystallization and magnetism of the thin films. It was established that the crystallization of a film at $T_S = 800$ °C is the best, and the saturation magnetization reaches 172.5 emu/cc. The coercivity of films at $T_S = 600$ °C reaches 15 kOe affected by film stress and oxygen vacancies, which is reportedly the maximum value in $(1-x)Fe_2O_3 - xFeTiO_3$. Thereafter, it decreases rapidly with the increase in T_S, resulting in lattice relaxation, stress reduction, and coercivity reduction. Oxygen vacancies affect the electrical properties in thin films. In contrast to bulk materials, we established that the conduction mechanism of films changes from thermally activated transition to programmed transition with decreasing temperature.

Keywords Ferromagnetic semiconductor · Hemo–Ilmenite film · Oxygen vacancy

1 Introduction

Compared with conventional semiconductor devices, spintronic devices using both charge and spin properties of electrons have the advantages of high speed and large storage. Therefore, magnetic semiconductor materials with both magnetic and semiconductor transport properties have a wide prospect in application in the field of spintronics [1–3], which is also a crucial problem to be solved in the novel generation of spintronic devices. Hematite has a distribution of Fe^{3+} with a modulation length of 2 layers and ilmenite has a distribution of Fe^{2+} with a modulation length of 4 layers. This leads to complex magnetic interactions in the solid solutions; therefore, solid solutions of hematite and ilmenite (Hemo–Ilmenite, HI) are useful for investigating mixed-spin oxide systems [4–7].

The solid solution $(1-x)Fe_2O_3 - xFeTiO_3$ $(0 < x < 1)$ is widely studied as a natural magnetic semiconductor material in the preparation of many oxides on an α-Al_2O_3(001) substrate by changing the substrate temperature (T_S) [8–11]. Magnetization jumps and the exchange bias effect are simultaneously observed in the oxide $(\alpha\text{-}Fe_2O_3)_{0.1}$–$(FeTiO_3)_{0.9}$ of bulk materials at 2.0 K [12, 13]. Ilmenite ($FeTiO_3$) and hematite (Fe_2O_3) are antiferromagnetic insulators. They have a hexagonal structure, in which oxygen ions are arranged in hexagonal dense packing lattice and 2/3 of the octahedral gap is occupied by cations. Fe^{2+} and Ti^{4+} layers are interlaced in $FeTiO_3$, and the space group is $R\bar{3}$. However, Fe^{3+} replaces Fe^{2+} and Ti^{4+} layers in Fe_2O_3, and the space groups become $R\bar{3}c$. HI $(1-x)Fe_2O_3 - xFeTiO_3 (0 < x < 1)$ has ordered $R\bar{3}$ and disordered $R\bar{3}c$ construction [14]. Many people believe that the magnetism of HI is closely related to the ordered structure [15–18]. Notably, only films with ordered structure can acquire strong ferromagnetism. The

✉ Liyun Jia
jliyun@126.com

✉ Denglu Hou
houdenglu@mail.hebtu.edu.cn

[1] Department of Mathematics and Physics, Hebei University of Architecture, Zhangjiakou 075000, China

[2] College of Physics, Hebei Normal University, Shijiazhuang 050024, China

[3] Hebei Nangong Middle School Xingtai, Xingtai 055750, China

magnetic moment of the film prepared by Dou et al. is close to that of the bulk sample, but it was not proved whether the film has an ordered structure [19]. The ordered HI film with $x=0.7$ prepared by Hojo et al. has the same weak magnetism as the disordered structure [20]. The ordered structure of the film is usually determined by the appearance of the diffraction peaks (003) and (009) in an X-ray diffraction (XRD) chart. The complex magnetic interactions in the bulk sample of HI are mainly determined by the ordered structure, but the factors affecting magnetism are different in thin films.

Through PLD and by adjusting T_S, we prepared epitaxial $Fe_{1.1}Ti_{0.9}O_{3-\delta}$(HI-9) thin films and demonstrated the effects of T_S on the structure, surface morphology, optical properties, magnetic properties, and electrical properties of the thin films.

2 Experimental Methods

For PLD, thin epitaxial $Fe_{1.1}Ti_{0.9}O_{3-\delta}$ films were prepared in a substrate. PLD target is made of 90% $FeTiO_3$ powder and 10% Fe_2O_3 powder, which was fully mixed and ground, and then it was sintered using conventional solid reaction method. KrF pulse laser deposition was used in the experiment. The wavelength of the laser was 248 nm, the working frequency was 2 Hz, and the laser energy was 3 J/cm2. The intrinsic vacuum pressure of the PLD chamber was $5.0\times10-5$ Pa. The deposition atmosphere is Ar and the pressure was $1.0\times10-5$ Pa. The T_S was 600–900 °C, and the temperature interval was 100 °C. The distance between the target and the substrate was 3.5 cm, and the thickness of the film was 60 nm. After deposition, the film was annealed for 0.5 h and cooled to room temperature naturally with constant pressure.

The phase structure of the films was analyzed via XRD with Compex Pro205. The surface morphology of the films was observed via NanoScope IV atomic force microscopy (AFM). The optical properties of the films were measured using a UV-3600 ultraviolet and visible (UV/VIS) spectrophotometer produced by Shimadzu, Japan. The magnetic and electrical properties of the films were measured using a physical property measurement system (PPMS) made by Quantum Design company.

3 Results and Analysis

3.1 Phase Analysis

Figure 1(a) shows the XRD patterns of the films prepared under different T_S conditions. The diffraction peaks (006) and (0012) of the ordered $R\bar{3}$ and disordered $R\bar{3}$ structures can be observed in the figure, whereas diffraction peaks (003) and (009) of the ordered $R\bar{3}$ structure cannot be observed, which indicates that the films have a disordered structure. No other impure peaks were observed, which indicates that the films were well epitaxial. The intensity of diffraction peak (006) of the $T_S=600$ °C film is the weakest, and its crystallization is poor.

Figure 1(b) shows that the diffraction peak of (006) gradually moves to a small angle with increasing T_S, which indicates that the lattice constant, c, increases. However, the (006) diffraction peak of the $T_S=800$ °C films becomes abnormal, and c decreases as the

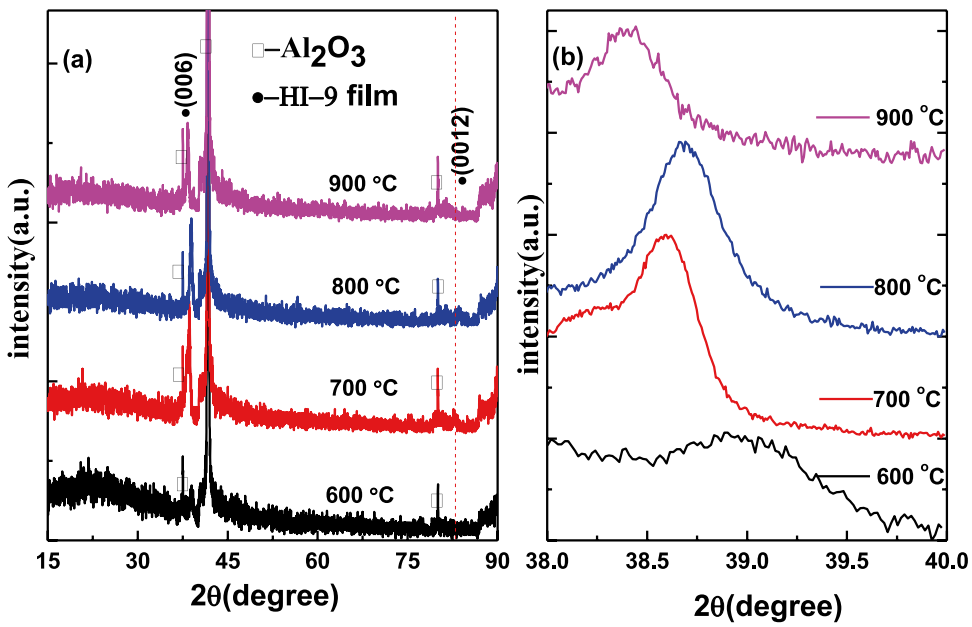

Fig. 1 (**a**) XRD diagram of the HI-9 thin films prepared under different T_S, boxes and black dots denotes the diffraction peak of Al_2O_3 and the film HI-9, respectively. (**b**) Magnified view of the diffraction peak of the film (006)

diffraction peak shifts to a larger angle. This is because of the increase of T_S, and thus the oxygen loss of the film increases, Fe^{3+} changes into Fe^{2+} (the radius of Fe^{2+} is larger than Fe^{3+}), and the Coulomb gravitational interaction of $Fe^{2+/3+} - O^{2-} - Fe^{2+/3+}$ changes into $Fe^{2+} - Fe^{2+}$ Coulomb repulsive interaction. The diffraction peak of the film prepared at $T_S = 800$ °C changes abnormally, and it could be owing to the following reasons: owing to lattice mismatch (HI bulk $a = 5.086$ Å, Al_2O_3 $a = 4.763$ Å), there is in-plane compressive stress in the film, T_S increases, lattice relaxation occurs, and c decreases. c decreases with the increase of crystallinity.

3.2 Analysis of the Surface Morphology of the Film

Figure 2 shows the AFM diagram of films prepared at different T_S. The scanning range is 1×1 μm. It is observed that the size of the film particles is uniform, and the particles gradually become larger with increasing T_S. The measured root mean square deviation (RMS) of the films prepared at $T_S = 600$–900 °C were 0.253, 0.228, 0.285, and 0.289 nm. RMS first decreases and then increases, but the difference is not significant, indicating that the film surface is smooth.

3.3 Analysis of the Optical Properties

The transmittance of the film samples was measured using a UV/VIS spectrophotometer in the wavelength range of 220–2600 nm. The absorptivity of sample was obtained using the transmittance of the film sample. The absorption coefficient of the sample is $\alpha = 2.303 \times A/t$, where t is the thickness of the film, A is the absorptivity of the film. α and the phonon energy, $h\upsilon$, of direct band gap semiconductor

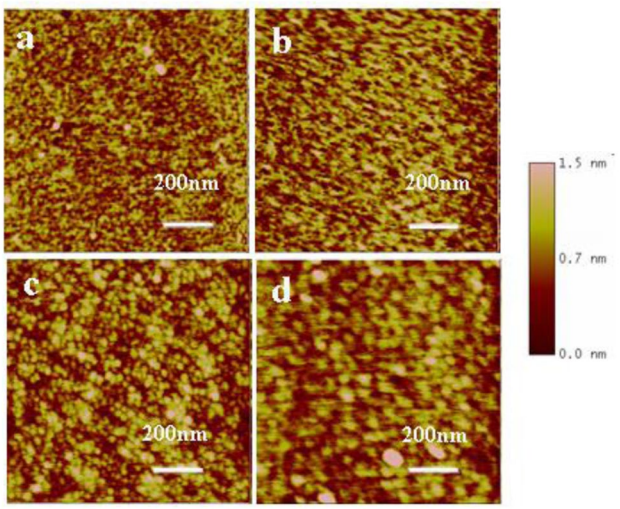

Fig. 2 Surface morphology of the HI-9 films prepared at different T_S, (**a**) $T_S = 600$ °C, (**b**) $T_S = 700$ °C, (**c**) $T_S = 800$ °C, and (**d**) $T_S = 900$ °C

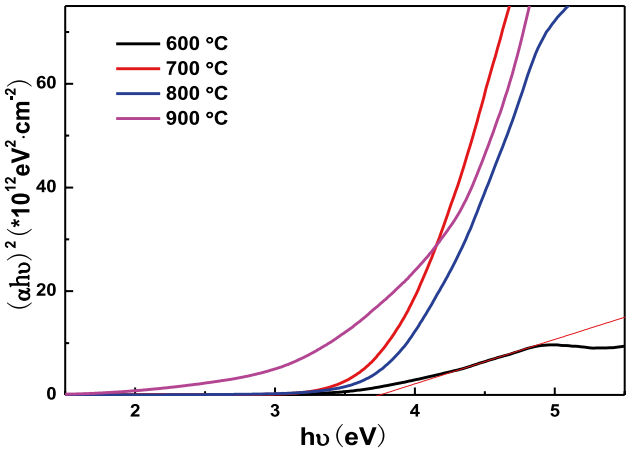

Fig. 3 $(\alpha h\upsilon)2$ varied diagram of the HI-9 thin films with the phonon energy $h\upsilon$ prepared at different T_S

satisfy the relative formula $(\alpha h\upsilon)^2 \approx (h\upsilon - E_g)$ [21]. According to this formula, we can calculate the optical band gap (E_g) of the thin film sample, that is, we can make a $(\alpha h\upsilon)^2 - h\upsilon$ graph according to the absorption coefficient of the sample, and then determine that E_g is the linear part of the extrapolated curve and the intersection point $(\alpha h\upsilon)^2 = 0$ of the coordinate axis $h\upsilon$.

Figure 3 shows the $(\alpha h\upsilon)2$ variation with $h\upsilon$ of thin films prepared at different T_S conditions. The results indicate that the films have a wide band gap. With the increase of T_S, the E_g of the film is 3.78, 3.87, 3.95, and 3.90 eV. The E_g of the film is wider than that of the pure $FeTiO_3$ film (3.55 eV) [21], which is consistent with the change of XRD. The films grown in Ar gas have more oxygen vacancies, and the E_g becomes larger, which is similar to literature reports [19]. The E_g of the films prepared at $T_S > 600$ °C was almost similar, and it was not affected by lattice relaxation (stress change), which indicates that the content of oxygen vacancy in the films is almost similar. The thin film at $T_S = 600$ °C has a relatively narrow E_g owing to low substrate temperature, much oxygen loss, and oxygen vacancy.

3.4 Analysis of the Magnetic Properties

Figure 4 shows the varied curves of coercivity and saturation magnetization of the thin film sample with T_S, which the magnetic field is parallel to the film surface. The figure shows that the coercivity of the film at $T_S = 600$ °C is 15 KOe, and it decreases rapidly with the increase in T_S. Notably, anisotropy, oxygen vacancy, and stress affect the coercivity of thin films mainly. According to the previous analysis of the E_g, oxygen vacancy content in the films prepared at $T_S > 600$ °C is the same; therefore, the effect of oxygen vacancy on the coercivity of the films is similar. However, the film prepared at $T_S = 600$ °C has less oxygen

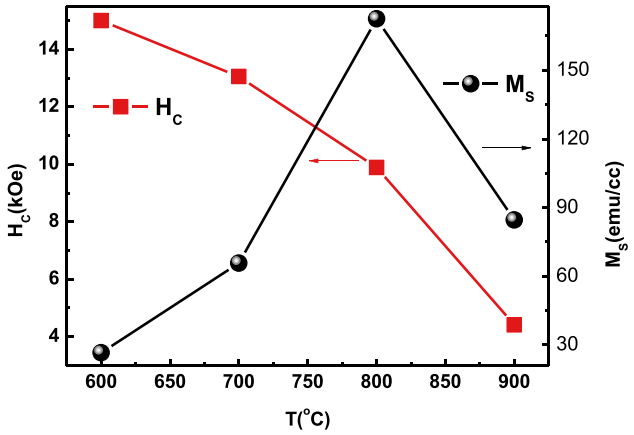

Fig. 4 Curve of coercivity and saturation magnetization at 5 K

loss and oxygen vacancy, and the in-plane compressive stress of the film is the largest. Therefore, the stress in the HI-9 film sample has a significant influence on the coercivity of the film. Lattice relaxation occurs with the increase of T_S, and then the stress decreases gradually, and the coercivity decreases rapidly. Similar to the previous analysis in XRD, the film prepared at $T_S = 600$ °C has poor crystallization; therefore, its magnetism is the weakest. With the increase in T_S, the crystallization of the film gradually increases. The crystallization of the film prepared at $T_S = 800$ °C is the best, and the saturation magnetization (Ms) reaches 172.5 emu/cc.

3.5 Measurement of the Electrical Properties of the HI-9

As shown in Fig. 5, the film at $T_S = 600$ °C is not conductive, which is because of the poor crystallization of the film. In contrary, the film at $T_S = 700$, 800, or 900 °C can conduct electricity. The resistivity of the film increases with the decrease in temperature, indicating that the film has semiconductor conductivity. In addition, the resistivity of the film at $T_S = 800$ °C is the lowest, and the resistivity of the film at $T_S = 700$ °C is slightly lower than that of the film at $T_S = 900$ °C film, which is consistent with the rule of Ms changing with T_S. This indicates that the film at $T_S = 800$ °C has a high degree of order, and the resistivity of the film is smaller than that of the HI-9 bulk sample, which is owing to the oxygen vacancy in the hypoxia film, and it changes Fe^{3+} into Fe^{2+}. We established that the conductivity of the film satisfies the Arrhenius conduction mechanism, $\sigma = \sigma_0 \exp(-E/2kT)$, at high temperature, where E is the activation energy, k is the Boltzmann constant, and σ_0 is the prefactor [22]. When the temperature is low, the film satisfies both the Mott program transition and the Arrhenius conduction mechanism,$\sigma = \sigma_1 \exp[-(T_1/T)^{0.5}] + \sigma_2(E/2kT)$, where T_1 is the characteristic temperature [17]. Figure 5 inset shows the conductivity curve of the film at $T_S = 800$ °C as a function of temperature, which is consistent with both the Mott program transition and the Arrhenius conduction mechanism. That is, at the critical temperature, the conduction mechanism of the film changes from a thermally

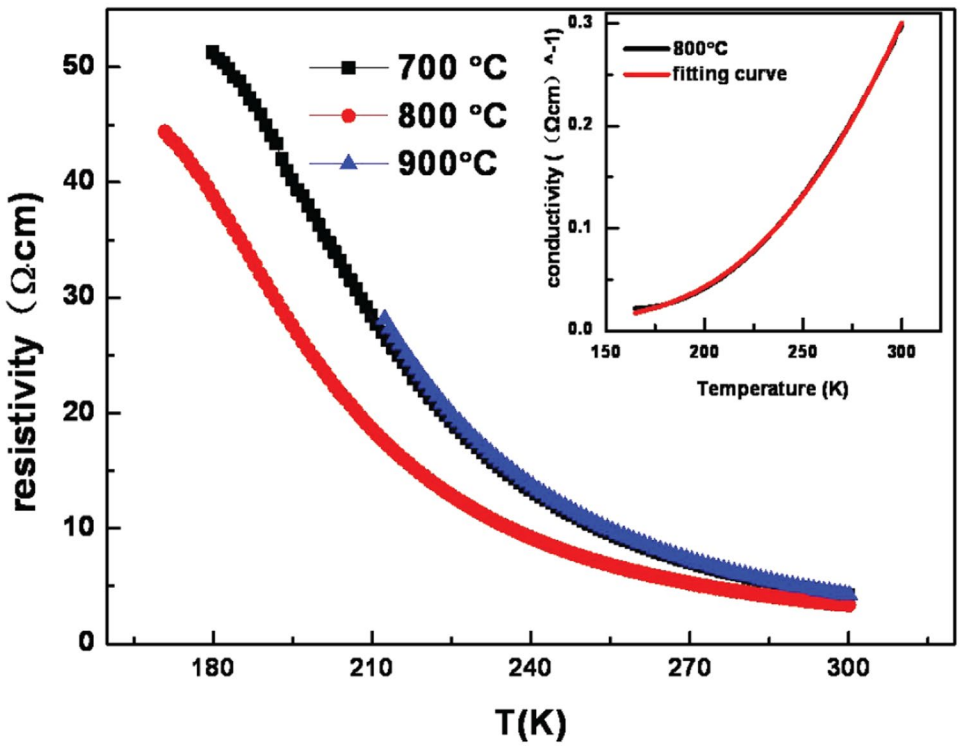

Fig. 5 Resistivity curves of the films at $T_S = 700$, 800, and 900 °C varied with temperature; fitting diagram of the conductivity of the film at $T_S = 800$ °C

activated transition to a programmatic transition, which indicates that the carriers of the film are localized at low temperature. The critical temperatures of the films at $T_S = 700$ and 800 °C are 208 and 195 K, respectively. A minimum activation energy of 102.15 meV is required for the thermal activation transition of the film at $T_S = 800$ °C, and the minimum activation energies of the films at $T_S = 700$ and 900 °C are 114.95 and 114.30 meV.

The resistivity curve of the HI-9 bulk sample under different magnetic fields varies with temperature (Fig. 6). The figure shows that the resistivity of the HI-9 bulk sample increases gradually with the decrease in temperature, indicating significant semiconductor characteristics. As shown by the arrow in Fig. 6(a), the resistance shows a clear turning point at 60 K, which is consistent with the magnetic ordered transition temperature of Fe^{2+}. Below 60 K, the spin of Fe^{2+} is antiparallel. At the same temperature, the resistance decreases gradually with the increase in external magnetic field. We can use the Arrhenius conduction mechanism to fit the conductivity with temperature variation under zero magnetic field, the expression is $\sigma = \sigma_0 \exp(-E/2kT)$ [22], as same as the films with high temperature. As shown in Fig. 6(b), the conductivity of the HI-9 bulk follows the thermal activation conductive mechanism, and the activation energy is 117.55 meV.

The resistivity of the thin film samples increases with the decrease in temperature and it has significant semiconductor conductivity. We also prepared Hi-9 films in the oxygen environment. It was found that the films showed the characteristics of insulators when the oxygen pressure was high, and the films were conductive only when the oxygen pressure was low. The resistivity of the film samples increased with the increase of oxygen pressure. The conductivity of the films prepared at low oxygen pressure is better than that of the HI-9 bulk sample, and the phenomenon is similar for $FeTiO_{3\pm\delta}$ [23] and $Fe_{1.5}Ti_{0.5}O_{3\pm\delta}$ [24]. The conductivity of the sample can be enhanced when cations of the same element appear in multiple valence states [25]. As the oxygen pressure decreases, oxygen vacancies form in the films, and some Fe^{3+} become Fe^{2+}. The change in oxygen vacancy and Fe valence state is the main reason for the change in electrical conductivity. The resistivity of the film we prepared is relatively high, as compared with the resistivity of the HI-9 film prepared by Zhou et al. (3.93 Ω cm) [26]. This phenomenon is also found in many other oxides [27]; therefore, oxygen vacancies are crucial for the HI solid solution systems.

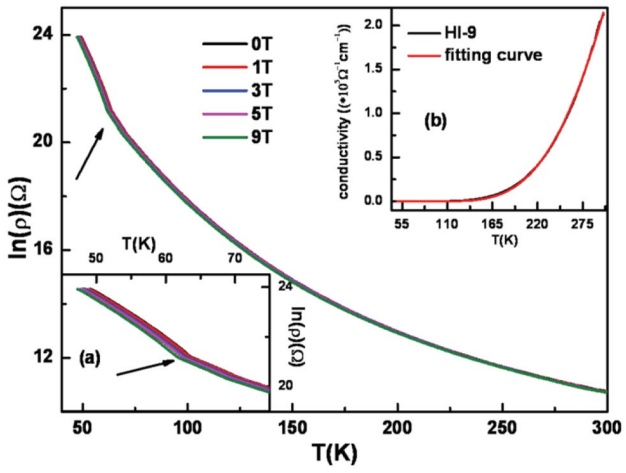

Fig. 6 lnρ-T plots of the HI-9 bulk sample measured at different magnetic fields; (**a**) a local enlargement of the lnρ-T plots; (**b**) a conductivity fitting plot

Contrast the HI-9 bulk sample, we established that the conduction mechanism of the film changes from the thermal activation transition to the variable-range hopping with decreasing temperature, which indicates that the carriers of films are localized at low temperature. Oxygen vacancies cause the changes of electrical properties. Magnetic and electrical measurements show that the film at $T_S = 800$ °C has the highest saturation magnetization and the best electrical conductivity, indicating that it has a relatively high degree of order, and its rule of the saturation magnetization, remanent magnetization, and coercivity changes consistently with those of the bulk material.

In HI-9 system, antiferromagnetic Fe^{3+} clusters are nested in antiferromagnetic Fe^{2+} lattices and form a triangular lattice. In this structure, 2/3 of the magnetic moments, all Fe^{3+} cations, order antiferromagnetically with each other. The remaining 1/3, all Fe^{2+} cations, are "confused." This structure forms a partially disordered antiferromagnetic state. The partially disordered antiferromagnetic state transforms into a ferromagnetic state, and it will induce the antiferromagnetic spins of the Fe^{2+} ions to enter a ferromagnetic state, resulting in the optical and transport properties of Hi-9 [12].

4 Conclusion

In this study, $Fe_{1.1}Ti_{0.9}O_{3-\delta}$ thin films were prepared on an α-Al_2O_3 (001) substrate and in Ar gas via PLD. The thin films are epitaxial growing with a symmetrical structure and a smooth surface. By measuring and analyzing the optical and magnetic properties of the thin films, we established that there were more oxygen vacancies in the thin films prepared in Ar atmosphere, and the E_g of the thin films widened significantly. T_S has a significant influence on the crystallization and magnetism of thin films. The crystallization of the films prepared at $T_S = 800$ °C is the best, and the saturation magnetization reaches 172.5 emu/cc. As the T_S increases, the stress decreases and lattice relaxation occurs. The coercivity

of the film decreases rapidly from 15 to 4.4 kOe. Oxygen vacancies and stress affected the optical, magnetic, and electrical properties of the films.

Funding This work was supported by the National Natural Science Foundation of China (Grant No. 51971087) and funded by the Science and Technology Project of Hebei Education Department (Grant No. ZD2021040), the Department of Science and Technology of Hebei Province Scientific and Technological Research Project (Grant No. 15211036), and the science and technology plan projects of Zhangjiakou City (Grant No. 1611070A). National Natural Science Foundation of China,51971087,Li Ma,Funded by Science and Technology Project of Hebei Education Department,ZD2021040,Liyun Jia,the Department of Science and Technology of Hebei Province Scientific and Technological Research Project,15211036,Jialing Xu,he financial support from science and technology plan projects of Zhangjiakou City,1611070A,Jialing Xu

References

1. Dietl, T., Ohno, H.: Ferromagnetic III–V and II–VI semiconductors. MRS Bull. **28**(10), 714–719 (2003). https://doi.org/10.1557/mrs2003.211
2. Chambers, S.A., Farrow, R.F.C.: New possibilities for ferromagnetic semiconductors. MRS Bull. **28**(10), 729–733 (2003). https://doi.org/10.1557/mrs2003.214
3. Molnar, S.V., Read, D.: New materials for semiconductor spin-electronics. Proc. IEEE **91**(5), 715–726 (2003). https://doi.org/10.1109/JPROC.2003.811803
4. Charilaou, M., et al.: Interaction-induced partitioning and magnetization jumps in the mixed-spin oxide $FeTiO_3$-Fe_2O_3. Phys. Rev. Lett. **107**(5), 057202 (2011). https://doi.org/10.1103/PhysRevLett.107.057202
5. Meng, X.Y., et al.: Enhanced photoelectrochemical activity for Cu and Ti doped hematite: the first principles calculations. Appl. Phys. Lett. **98**(11), 112104 (2011). https://doi.org/10.1063/1.3567766
6. Charilaou, M., et al.: Large spontaneous magnetostriction in $FeTiO_3$ and adjustable magnetic configuration in Fe(III)-doped $FeTiO_3$. Phys. Rev. B **86**(2), 024439 (2012). https://doi.org/10.1103/PhysRevB.86.024439
7. Moure, C., Peña, O.: Magnetic features in $REMeO_3$ perovskites and their solid solutions (RE=rare-earth, Me=Mn, Cr). J. Magn. Magn. Mater. **337–338**, 1–22 (2013). https://doi.org/10.1016/j.jmmm.2013.02.022
8. Ishikawa, Y., Akimoto, S.-I.: Magnetic properties of the $FeTiO_3$-Fe_2O_3 solid solution series. J. Phys. Soc. Jpn. **12**(10), 1083–1098 (1957). https://doi.org/10.1143/JPSJ.12.1083
9. Ishikawa, Y.: Magnetic properties of ilmenite-hematite system at low temperature. J. Phys. Soc. Jpn. **17**(12), 1835–1843 (1962). https://doi.org/10.1143/JPSJ.17.1835
10. Hojo, H., et al.: Magnetic structures of $FeTiO_3$-Fe_2O_3 solid solution thin films studied by soft X-ray magnetic circular dichroism and ab initio multiplet calculations. Appl. Phys. Lett. **104**(11), 112408 (2014). https://doi.org/10.1063/1.4868638
11. Fujii, T., et al.: Microstructural properties of (11$\bar{2}$0)-oriented hematite–ilmenite solid solution films. Thin Solid Films **591**, 245–249 (2015). https://doi.org/10.1016/j.tsf.2015.04.028
12. Song, P., et al.: *Magnetization jumps and exchange bias induced by a partially disordered antiferromagnetic state in* $(FeTiO_3)_{0.9}$-$(Fe_2O_3)_{0.1}$. J. Appl. Phys. **115**(21), 213907 (2014). https://doi.org/10.1103/PhysRevApplied.11.054018
13. Song, P., et al., *Dynamic magnetic-transformation-induced exchange bias in* $[\alpha\text{-}Fe_2O_3]_{0.1}$ $[FeTiO_3]_{0.9}$. Phys. Rev. Appl. **11**(5), 054018 (2019). https://doi.org/10.1103/PhysRevApplied.11.054018
14. McEnroe, S.A., et al.: Lamellar magnetism: effects of interface versus exchange interactions of nanoscale exsolutions in the ilmenite-hematite system. J. Phys: Conf. Ser. **17**, 154–167 (2005). https://doi.org/10.1088/1742-6596/17/1/022
15. Hojo, H., et al., *Room-temperature ferrimagnetic semiconductor* $0.6FeTiO_3{\cdot}0.4Fe_2O_3$ *solid solution thin films.* Appl. Phys. Lett. **89**(14), 142503 (2006). https://doi.org/10.1063/1.2357547
16. Hamie, A., et al.: Structural, optical, and magnetic properties of the ferromagnetic semiconductor hematite-ilmenite $Fe_{2-x}Ti_xO_{3-\delta}$ thin films on $SrTiO_3$(001) prepared by pulsed laser deposition. J. Appl. Phys. **108**(9), 093710 (2010). https://doi.org/10.1063/1.3501104
17. Matoba, T., et al.: Low-temperature growth of highly crystallized $FeTiO_3$-Fe_2O_3 solid solution thin films with smooth surface morphology. J. Phys: Conf. Ser. **200**(6), 062011 (2010). https://doi.org/10.1088/1742-6596/200/6/062011
18. Chambers, S.A.: Ferromagnetism in doped thin-film oxide and nitride semiconductors and dielectrics. Surf. Sci. Rep. **61**(8), 345–381 (2006). https://doi.org/10.1016/j.surfrep.2006.05.001
19. Dou, J., et al.: Preparation and characterization of epitaxial ilmenite-hematite films. J. Appl. Phys. **101**(5), 053908 (2007). https://doi.org/10.1063/1.2450678
20. Hojo, H., et al.: Epitaxial growth of room-temperature ferrimagnetic semiconductor thin films based on the ilmenite-hematite solid solution. Appl. Phys. Lett. **89**(8), 082509 (2006). https://doi.org/10.1063/1.2337276
21. Dai, Z., et al.: Structural, optical, and electrical properties of laser deposited $FeTiO_3$ films on C- and A-cut sapphire substrates. J. Appl. Phys. **85**(10), 7433–7437 (1999). https://doi.org/10.1063/1.369374
22. Bocher, L., et al., *Direct evidence of Fe2+Fe3+ charge ordering in the ferrimagnetic hematite-ilmenite* $Fe_{1.35}Ti_{0.65}O_{3-\delta}$ *thin films.* Appl. Phys. Lett. **111**(16), 167202 (2013). https://doi.org/10.1103/PhysRevLett.111.167202
23. Popova, E., et al.: Systematic investigation of the growth and structural properties of $FeTiO_{3\pm\delta}$ epitaxial thin films. J. Appl. Phys. **103**(9), 093909 (2008). https://doi.org/10.1063/1.2913346
24. Ndilimabaka, H., et al., *Magnetic and transport properties of the room-temperature ferrimagnetic semiconductor* $Fe_{1.5}Ti_{0.5}O_{3\pm\delta}$*: influence of oxygen stoichiometry.* J. Appl. Phys. **103**(7), 07D137 (2008). https://doi.org/10.1063/1.2835479
25. Ishikawa, Y.: Electrical properties of $FeTiO_3$-Fe_2O_3 solid solution series. J. Phys. Soc. Jpn. **13**(1), 37–42 (1958). https://doi.org/10.1143/JPSJ.13.37
26. Zhou, F., Kotru, S., Pandey, R.K.: Pulsed laser-deposited ilmenite–hematite films for application in high-temperature electronics. Thin Solid Films **408**(1), 33–36 (2002). https://doi.org/10.1016/S0040-6090(02)00075-5
27. Dumont, Y., et al.: Tuning magnetic properties with off-stoichiometry in oxide thin films: an experiment with yttrium iron garnet as a model system. Phys. Rev. B **76**(10), 104413 (2007). https://doi.org/10.1103/PhysRevB.76.104413